The early Ediacaran *Caveasphaera* foreshadows the evolutionary origin of animal-like embryology

Zongjun Yin[1†*], Kelly Vargas[2†], John Cunningham[2], Stefan Bengtson[3], Maoyan Zhu[1], Federica Marone[4], Philip Donoghue[2*]

*authors for correspondence | †authors contributed equally to the study

[1]State Key Laboratory of Palaeobiology and Stratigraphy, Nanjing Institute of Geology and Palaeontology & Center for Excellence in Life and Paleoenvironment, Chinese Academy of Sciences, Nanjing 210008, China.

[2]School of Earth Sciences, University of Bristol, Life Sciences Building, Tyndall Avenue, Bristol BS8 1TQ, UK.

[3]Department of Palaeobiology, Swedish Museum of Natural History, Box 50007, SE-104 05, Stockholm SE, Sweden

[4]Swiss Light Source, Paul Scherrer Institute, CH-5232 Villigen, Switzerland

*Corresponding authors: zjyin@nigpas.ac.cn; phil.donoghue@bristol.ac.uk

Lead Contact: Philip Donoghue (phil.donoghue@bristol.ac.uk)

SUMMARY

The Ediacaran Weng'an Biota (Doushantuo Formation, 609 million years old) is a rich microfossil assemblage that preserves biological structure to a subcellular level of fidelity and encompasses a range of developmental stages [1]. However, the animal embryo interpretation of the main components of the biota has been the subject of controversy [2, 3]. Here we describe the development of *Caveasphaera*, which varies in morphology from lensoid, to a hollow spheroidal cage [4], to a solid spheroid [5], but has largely evaded description and interpretation. *Caveasphaera* is demonstrably cellular and develops within an envelope by cell division and migration, first defining the spheroidal perimeter via anastomosing cell masses that thicken and ingress as strands of cells that detach and subsequently aggregate in the polar region. Concomitantly, the overall diameter increases as does the volume of the cell mass but, after an initial phase of reductive palinotomy, the volume of individual cells remains the same through development. The process of cell ingression, detachment and polar aggregation is analogous to gastrulation; together with evidence of functional cell adhesion and development within an envelope, this is suggestive of a holozoan affinity. Maternal investment in the embryonic development of *Caveasphaera* and co-occuring *Tianzhushania* and *Spiralicellula*, as well as delayed onset of later development, may reflect an adaptation to the heterogeneous nature of the early Ediacaran nearshore marine environments in which early animals evolved.

RESULTS

The Weng'an biota provides a unique insight into multicellular life in the early Ediacaran period during which molecular clocks estimate the fundamental animal lineages to have diverged [6]. Indeed, there are numerous claims of animal remains from the biota, including miniature adult eumetazoans [7] and bilaterians [8], and embryonic animals [2, 9-12], but all remain contentious [3, 13-18]. However, there is a broader diversity of fossil remains from this deposit that have been the subject of little attention, some of which may have a greater claim on animal affinity. These fossils include *Caveasphaera costata* (Figure 1) which has been described as a spherical hollow cage (Figure 1A-C) [4] to a more solid sphere (Figure 1D) [5] of unknown nature and affinity, though superficial comparison has been drawn to embryos of an octocoral [4]. Analysis of the structure and development of *Caveasphaera* is challenging because of its small size and complex morphology. We employed Synchrotron Radiation X-ray Tomographic Microscopy (srXTM) [19] and High resolution X-ray microtomography [20] to analyse 233 specimens of *Caveasphaera* that encompass its morphological and size range, based on a rich fossil assemblage from '54' and Datang quarries in the Baiyan-Gaoping Anticline of Weng'an County, Guizhou Province, South China [21].

The cage-like and solid morphs have been interpreted to reflect intraspecific variation [5] but instead represent members of a more continuous spectrum of morphological variation (Figures 1, 2). *Caveasphaera* is a rare component of the Weng'an Biota, distinguished by its comparatively small cells, organised into a distinctive hollow spheroidal cage delimited by branching strands of cells and radial cell strands (Figures 1, 2). Earlier stages are lensoidal but can be associated reliably because they are composed of cells of similar phenotype and exhibit the characteristic arrangement of polarised and branching cell masses (Figures 1A, 2A-B). The latest stages identified are increasingly solid but can be associated based on their transitional continuum with earlier hollow stages (Figure 2C-R). Although there is some taphonomic variation within the assemblage, 70 specimens are preserved in high fidelity (Figures 1, 2), demonstrating a cellular composition in which polygonal cells are closely-packed with Y-shaped interfaces (Figures 1E, F, 2U-Z). Quantitative computed tomography of the srXTM data demonstrates little variation in the volume of component cells within any one specimen and across development (Figure 3A) - with the exception of the lensoidal stages which have larger and fewer cells (Figure 1A, E). Across the range of specimens there is an almost two-fold (373 to 735 μm) increase in diameter and a more than eight-fold increase in the sum volume of cells (0.0171 to 0.2 mm^3) (Figure 3B, the raw data for Figure 3 is available in Data S1).

Almost all of the specimens of *Caveasphaera* in our collection lack an enclosing envelope and for most of the specimens with an envelope it is difficult to exclude the possibility that the association is taphonomic (e.g. Figure S1K, L). The paucity of specimens preserving an envelope is a reflection of the practical challenge of attributing specimens to *Caveasphaera* when their morphology is obscured by an envelope. Nevertheless, a small number of specimens representative of early and late stages of development are preserved in association with incomplete envelopes (Figure 1C, D; Figure S1A-J) and the broken openings into these are too small to support a *post mortem* taphonomic association. The envelopes range in diameter from 504 to 806 μm and, when completely preserved, have two layers, the outermost of which has an approximately polygonal verrucose ornament reminiscent of the 'Megasphaera' taphomorph of *Tianzhushania* (Figure S1C, D, G, H); this is more often lost taphonomically revealing the smooth and featureless inner layer (Figure 1C, D; Figure S1E, F, I) as is common with other embryo-like fossils from the Weng'an Biota [22]. The thickness of the inner envelope varies with the degree of void-filling diagenetic mineralization (compare Figure S1E, F, I versus J-L).

The specimens with among the lowest aggregate volume of cells have a lensoidal morphology with one smooth convex surface and another from which cellular protuberances emerge (Figures 1A, 2A, B). The smallest hollow spheroidal specimens are comprised of an interconnected network of anastomosing branches that show evidence of bifurcation, coalescence, and radial ingression (Figures 1B; 2C, D, K, L). The branching meshwork of cells defining the perimeter increases in size across specimens of progressive development (Figures 1A, B, 2A-C *vs* Figures 2E, F, M, N), and shows branching within this plane as well as radially towards the centre where it occupies the volume defined by the perimeter, as evidenced by laterally and internally protruding 'tails' (Figures 1A, 2C-E, K-M, O, U, W, 4C, D; Figure S2B, F). Consequently, the spheroidal perimeter is more continuous, with fewer and smaller openings to the interior (Figures 2G-J); the depth of the perimeter cell layer also increases (Figure 2K, L vs Figure 2N-Q). However, while the outer surface of the cell mass is smooth and convex, the inner surface is generally concave and irregular (Figure 2M, O, P), as a consequence of inwardly extending strands of cells (Figure 2U, W). In part, this appears to reflect ingression of cells and cell clusters, from the inner surface of the circumferential cell mass. This appears to have occurred individually, as evidenced by the development of constrictions in the radial cell strands to define barely attached cell clusters (Figure 2L, M, T, U), as well as isolated cell clusters which occur only within the lumen (Figures 4A-D, I, J; S2A-L). While taphonomy experiments have shown that cells within cleavage and gastrula embryos can lose adhesion *post mortem* [23], cell ingression seems to have occurred *in vivo* in *Caveasphaera* since there is direct evidence of cell masses coalescing (Figure 2L, T) which occurs in parallel with polar thickening of the cortex of cells, resulting in a thick-based, approximately cup-shaped body that reaches up around 80%-90% of the spheroid volume (Figure 2F, I, N, Q). Our largest specimen is an almost solid spheroid of cells preserving evidence of the infilling of the central void with cells (Figure 2J, R, Z). There is no evidence of the cell phenotype differentiation seen in other multicellular organisms in the Weng'an Biota [3, 24], nor do we have specimens representative of what must be the very earliest stages of development, comprised of few cells.

Among our collection of specimens, the aggregate volume of cells comprising specimens increases broadly and continuously with size (Figure 3B). Aside from the lensoidal stage (Figures 1A, 2A, B), the average volume of individual cells shows little variation between those in the centre of the body versus the perimeter (mean and standard deviation of 2881 μm^3 and 1318 μm^3 versus 3197 μm^3 and 1288 μm^3, respectively). There is no explicit correlation between specimen and cell size variables, and the volume of individual cells remains in a similar range among specimens from different size classes (Figure 3A). These facts require that the increase in the aggregate volume of cells among

specimens is achieved largely through cell addition, rather than through increase in the volume of individual cells (Figure 3B). Additional cells must have emerged through cell division and growth; as this is not observed it must have occurred at the time of cell division. Some of this variance in aggregate cell volume can be accounted for as a taphonomic artefact or developmental variation since many of the specimens we studied preserve cell aggregates that are isolated from the larger cell mass, preserved *in situ* within the central void as a consequence of geological mineralization (Figure 4A-D, Figure S2; their topology requires that they were held in place by a non-cellular matrix in vivo, this non-cellular matrix has been preserved in some specimens, for example Figures 4E-H, K-L, S3). The isolated cell clusters occur across the size range of specimens and range in number from 1 to 26, with most specimens preserving fewer than 10. Hence, it is likely that the aggregate volume of cells in many of the lower-density cage-like specimens is reduced as a consequence of the loss of isolated cell clusters *post mortem*. Nevertheless, these isolated cell clusters evidence a process by which the hollow stages develop into their denser, larger counterparts.

The presence of an outer envelope is potentially difficult to rationalise since it requires that the development of *Caveasphaera* (Figure 3C), with a greater than eight-fold increase in volume across specimens in our collection (Figure 3B), proceeded without an external source of nutrients. This contrasts with the pattern of development exhibited by *Tianzhushania* and *Spiralicellula* from the same deposit, which exhibit a more approximately constant volume across a pattern of binary reductive palintomy [3, 25]. This could be rationalised in *Caveasphaera* if the true pattern of development is the reverse of that described in Figure 3C, where the larger, denser specimens represent the earliest stages and development proceeds through the loss of cells, perhaps as propagules or gametes, detaching first from the interior as individual cells and clusters, with the overall cell mass reshaping and resizing through this process. However, the enclosing envelope makes this interpretation unlikely, if not impossible, since the expectation of hundreds of loose cells entrained within the envelope but outside the lumen, is not met. The difference in cell size between the lensoidal and spheroidal morphs also strongly suggests that they represent early and later stages, respectively. *Tianzhushania* and *Spiralicellula* both preserve evidence of intracellular lipids in specimens representative of the first few rounds of palintomy [17], but these cells are orders of magnitude larger than the cells of *Caveasphaera*; comparably-sized cells representative of later stages of palintomy show no such evidence. Nevertheless, two specimens of *Caveasphaera* preserve an extracellular matrix containing spheroidal structures that are smaller than the polygonal cells (Figure 4E-H, K, L; Figure S3). These exhibit comparable preservation to the structures interpreted as intracellular lipid droplets in *Tianzhushania* and *Spiralicellula* [17, 25], suggesting that these

developmental stages of *Caveasphaera* may have been invested in extracellular lipids that sustained growth and development within the closed, enveloped environment.

DISCUSSION

The multicelled organisation of *Caveasphaera* invites comparison to prokaryotes and eukaryotes with multicellular stages in their life cycles. The branching arrangement of cell masses seen in the cyanobacterium *Microcystis* [26, 27] are particularly reminiscent of *Caveasphaera*, but *Microcystis* does not comprise spheroids in this planktonic conformation [28]. Like other prokaryote multicellular colonies, *Microcystis* lacks the enclosing envelope of *Caveasphaera*; the cells are physically separate, bound together (through aggregation or vegetative association [29]) by mucilage [30], and so the cells do not exhibit the Y-shaped intercell junctions seen in *Caveasphaera* which are indicative of cell adhesion. Bacterial cysts form from thickening of the cell wall but are unicellular. Bacterial endospores are usually singular, forming within the mother cell wall; exceptionally up to nine endospores can form per cell [31] but even in such circumstances the endospores do not exhibit the Y-shaped intercell conformation exhibited by *Caveasphaera*. Indeed, Y-shaped intercell junctions are commonly interpreted to reflect flexible cell membranes and functional cell adhesion indicative of tissue-grade multicellularity and, specifically, an animal affinity [1, 2, 32, 33]. However, diverse eukaryotes exhibit multicellular stages in their lifecycles [34], many of which have cells arranged with Y-shaped intercell junctions [35]. Since multicellularity has evolved many times among extant eukaryotes, *Caveasphaera* might belong to any one of these living or (likely many more) extinct lineages of multicellular eukaryotes.

For example, apicomplexans such as *Perkinsus* also possess multicellular hypnospores and zoospores encapsulated within a cyst [36, 37], as do the chlorophytes *Ulotrix* and *Chlorococcum*, whereas chlorophytes such as *Spirogyra* and dinophyceaecean dinoflagellates provide encysted hypnozygotes of comparable grade [38]. Rhodophytes such as *Ptilothamnion* also produce polysporangiate spore masses that arise from repeated rounds of division beyond those that normally produce tetraspores [39]. Animals, plants, as well as red, brown and green algae all exhibit multicellular embryonic development [34]. The embryos of phaeophytes differentiate quickly, with rhizoid development apparent from before the first round of palintomy [40]; carpospore development in rhodophytes goes through more rounds of development but sporophyte morphogenesis is apparent within four or five rounds of palintomy [41, 42]. In both phaeophytes and rhodophytes, the embryos are initially naked, only subsequently developing an irregular mucilaginous sheath [43, 44]. Volvocine algae exhibit cellular differentiation, recurrent rounds of palintomy, a process of inversion that resembles

patterns of gastrulation in some animals [45], and some volvocines also produce complex ornamented cysts [46]. However, the coordinated arrangement of cells in the multicellular zygotes of volvocines is achieved through incomplete cell division that appears ancestral [47].

None of these examples bear close comparison to *Caveasphaera* in that either their component cells are relatively small in number and uncoordinated (hypnospores, hypnozygotes and polysporangia), they lack a resting cyst and undergo rapid morphogenesis with only a single cell or a few tens of cells (phaeophyte embryos and rhodophyte carpospores), or they achieve cell coordination through incomplete cell division (volvocines). Much greater coordinated arrangement is exhibited by holozoans such as the ichthyosporeans *Creolimax*, *Pirium* and *Sphaeroforma* which, along with filastereans, possess a spheroidal multicellular stage comprised of tens to hundreds of cells with Y-shaped intercell junctions facilitated by functional cell adhesion [48]. Ichthyosporeans like *Sphaeroforma* develop initially as a multinucleate coenocyte [49] before undergoing cytokinesis to form a blastocoel-like structure with an epithelium-like perimeter of cells enclosed within an envelope [50-52]; the cells ultimately disaggregate and are released to the environment [52]. Thus, among eukaryotes that exhibit a multicellular embryo, spore or sporangial stage, the number of cells and patterns of cell adhesion and rearrangement inferred in the development of *Caveasphaera* bear close comparison only to the multicellular stages of non-metazoan holozoans and animal embryos. The arrangement of cells, defining an incomplete perimeter of the overall spheroid, is also seen in animal embryos [53, 54]. The overall arrangement of cells defining a perimeter around a central cavity is reminiscent of ichthyosporeans and the blastocoels of animal embryos. The inferred pattern of cell ingression, detachment and subsequent polar aggregation is comparable to gastrulation. Indeed, the pattern of branching cell masses is similar to the process of elongation associated with the developing gastrulae and planulae of cnidarians like *Hydractinia* [55], perhaps reflecting a similar process of embryonic development. Since the many alternative non-holozoan instances of convergently evolved aggregative or embryonic multicellularity are much more similar to one another than the more complex development of *Caveasphaera*, its similarities to holozoan and metazoan embryonic development are less likely to represent an extinct independent instantiation of embryonic multicellularity.

The developmental biology of *Caveasphaera* (Figure 3C) is more similar to the embryos of crown-metazoans than it is to outgroups including the choanoflagellates, filastereans, and ichthyosporeans (non-metazoan holozoans) (Figure 3D), all of which have a coordinated multicellular stage in what are otherwise unicellular life histories [56]. In large part, this is facilitated by the shared components

of what has been perceived to be a metazoan developmental toolkit of transcription factors, cell-adhesion and cell-signalling molecules [57], elements of which have been lost in filastereans and choanoflagellates [56, 57], reflecting lost ancestral complexity that may belie the distinctive complexity of metazoan bodyplans and their development, with respect to their holozoan [48] or opisthokont [58] ancestry. For this reason, we cannot discriminate the possibility that *Caveasphaera* was a close holozoan relative of metazoans from the possibility that it represents a stem- or crown-metazoan (Figure 3D). Therefore, we hold back on concluding that *Caveasphaera* evidences the origin of animals and their embryology, but it clearly indicates that processes similar to gastrulation, which is a shared primitive feature of metazoans [59], were present already by the early Ediacaran. In this regard, it is interesting that the development of *Caveasphaera* was invested in maternal resources, like the large and lipid rich *Tianzhushania* and *Spiralicellula*. This, together with the apparently delayed onset of later development – extending beyond thousands of cells - presumably reflects adaptation to the temporally and spatially heterogeneous nature of environmental conditions that prevailed in early Ediacaran nearshore marine environments [60]. In this sense, the attendant adverse geochemical environments do not appear to have constrained these formative steps in the evolutionary origins of animal complexity.

ACKNOWLEDGEMENTS

This study was supported by Strategic Priority Research Program (B) of the Chinese Academy of Sciences (CAS) (XDB 26000000 to YZ and MZ), Newton Advanced Fellowship (to YZ and PCJD), the Natural Environment Research Council (NE/P013678/1, to PCJD and YZ), National Natural Science Foundation of China (41672013 to YZ and PCJD) and the Youth Innovation Promotion Association of the CAS (2017360, to YZ). We also received funding from the European Union's Horizon 2020 research and innovation programme under grant agreement n.730872, project CALIPSOplus. Finally, we acknowledge the Paul Scherrer Institute, Villigen, Switzerland for provision of synchrotron radiation beamtime at the TOMCAT beamline of the Swiss Light Source.

AUTHOR CONTRIBUTIONS

PD and YZ designed the project and managed it to completion. SB, JC, PD, FM, KV, ZY collected the data, KV led the analysis of the data to which all authors contributed. PD, KV, ZY led both the interpretation of the results and the writing, to which all authors contributed.

DECLARATION OF INTERESTS

The authors declare no competing interests.

Figure 1. General biology of *Caveasphaera*.

(A, B), Naked specimens with cellular structure. (C, D), Specimens with envelopes. (E, F), close-up views of (A, B), respectively, showing detail of cellular structures. See also Figure S1. Scale bar: 85µm for (A), 95µm for (B), 130µm for (C), 90µm for (C), 40µm for (E), 38µm for (F). Tomographic models appear gold while scanning electron micrographs appear in greyscale.

Figure 2. Different developmental stages of *Caveasphaera*.

(A-J), Morphology of naked *Caveasphaera*. (K-R), Virtual slices of (C-J), respectively, showing internal structures. (S-Z), Close-up views of (K-M, O, P, R), respectively, showing cellular structure. The arrows in (U, W) indicate inwardly extending strands of cells. See also Figure S2. Scale bar: 200µm for (A, B), 120µm for (C, K), 130 for (D, L, N, Q), 160µm for (E), 155µm for (F), 118µm for (G), 176µm for (H), 145 for (I), 185 for (J), 150µm for (M), 114µm for (O), 154µm for (P), 177µm for (R), 43µm for (S), 27µm for (T), 33µm for (U), 21µm for (V, W), 26µm for (X), 20µm for (Y), 27µm for (Z).

Figure 3. Developmental biology and phylogenetic affinity of *Caveasphaera.*

(A) Box-plot of body diameter (diameter of naked spheroidal body of cell mass) and individual cell volume, showing little variation of cell volume/size across different specimens. Individual volume of cells (137 cells in total) were measured from 27 well-preserved specimens with clear cell boundaries (refer to Data S1 for raw data); (B) Non-linear relationship between body diameter and body volume (that is, the sum of cell volumes). The body diameter and volume were measured based on 100 unbroken specimens' segmented volume data (refer to Data S1 for raw data). The filled and unfilled circles represent specimens with and without cellular structures, respectively. The row of cartoons in (B) are stylized representations of the cross-sectional morphology of *Caveasphaera* at different developmental stages, reflecting the broad correlation between the size and morphology of these developmental stages. (C) *Caveapshaera* develops from small, hollow cage stages to larger solid stages within a two-layered envelope. (D) a simplified phylogenetic tree of Holozoa, with Holomycota as the outgroup [56]. LMCA= last metazoan common ancestor. UMCA=unicellular metazoan common ancestor. LHCA=last holozoan common ancestor. The potential placements for *Caveasphaera* in the holozoan tree are indicated in blue.

Figure 4. Specimens with isolated cell clusters and possible lipid droplets.

(A, C), Surface renderings, the cell clusters were indicated by red, cyan, green, pink, purple and blue. (B, D), Virtual three-dimensional sections of (A, C), respectively. (E, G), Surface renderings. (F, H),

Virtual slices of (E, G), respectively, showing preserved intercellular matrix. (I, J), Close-up views of (B), showing cellular structures of isolated cell cluster and cell mass. (K, L), Close-up views of (F, H), respectively, showing lipid-like vesicles (arrow heads). See also Figure S3. Scale bar: 150µm for (A), 140µm for (B), 110µm for (C, D), 85µm for (E, F), 120 µm for (G, H), 35µm for (I), 27µm for (J), 30µm for (K), 38µm for (L).

STAR Methods

LEAD CONTACTS AND MATERIALS AVAILABILTY

Further information and requests for resources and reagents should be directed to and will be fulfilled by the Lead Contacts, Philip Donoghue (phil.donoghue@bristol.ac.uk) and Zongjun Yin (zyin@nigpas.ac.cn).

EXPERIMENTAL MODEL AND SUBJECT DETAILS

The specimens described in this study are available at Nanjing Institute of Palaeontology and Stratigraphy Chinese Academy of Sciences (NIGPAS), Nanjing, China under collections numbers NIGP 171455 to 171680, and the Swedish Museum of Natural History, Box 50007, SE-104 05, Stockholm, Sweden under collections numbers NRM X8334 to X8340.

METHOD DETAILS

Specimen recovery

Specimens were recovered from rock samples from the Upper Phosphorites of the Datang and 54 quarries, Weng'an, Guizhou Province, China [21]. The carbonate constituents of the samples were dissolved in ca 8%-10% acetic acid and the phosphatised fossils were recovered from the resulting residues by manual sorting under a binocular microscope. Figured specimens are deposited at Nanjing Institute of Geology and Palaeontology, Chinese Academy of Sciences (NIGPAS). Selected specimens were also examined using a scanning electronic microscope (Leo VP1530) operating at voltage ranging from 5 to 20 KV.

Scanning Electron Microscopy

Selected specimens were also examined using a scanning electronic microscope (Leo VP1530) operating at voltage ranging from 5 to 20 kv, at the Nanjing Institute of Palaeontology and Stratigraphy, Chinese Academy of Sciences, Nanjing, China.

X-Ray and Computed Tomography

Tomographic scanning was carried out at the X02DA (TOMCAT) beamline of Swiss Light Source (Paul Scherrer Institute, Switzerland) and at the micro-CT lab of NIGPAS, using srXTM [19] and high-resolution X-ray microtomography [20]. The tomographic data were analysed using AVIZO and VG StudioMax (3.0) software. A three-dimensional model was reconstructed for each specimen and the body volume was calculated in Avizo or VG StudioMax from the segmented model. As the specimens are not perfect spheres, the diameter of *Caveasphaera* was calculated as the average of three (x, y, z) body measurements. 233 specimens were scanned and, 70 of them show well-preserved cellular structures (Data S1). Volume data for 100 unbroken specimens were segmented to measure the body diameter, number of isolated cell clusters and sum volume of cell mass. Based on the segmented volume data of the specimens showing the best cell preservation with clear membranes, individual volumes of 137 internal cells (within the main body) of 27 specimens across different developmental stages were measured, and 48 surface cells (in contact with the surface of the main body) of 8 specimens with different sizes were measured. Cell volumes were calculated in Avizo using the material statistics function.

QUANTIFICATION AND STATISTICAL ANALYSIS

Graphs and statistical analyses were performed using R [61].

DATA AND CODE AVAILABILITY

The tomographic datasets and associated computed tomographic models are available from Bristol University Research Data Repository https://data.bris.ac.uk/data/7eku32izrw5s2nrno2m0oxtj1

Data S1. Specimen and cell measurements. Related to Figure 3.

(A) Measurement of 137 cells from 27 specimens with different diameters. (B) Measurements of the sum cell volumes per specimen, the diameter of those specimens, and the preservation determination. (C) Diameter and volume of subsurface cells. (D) Diameter and volume of surface cells.

REFERENCES

1. Xiao, S.H., Muscente, A.D., Chen, L., Zhou, C., Schiffbauer, J.D., Wood, A.D., Polys, N.F., and Yuan, X.L. (2014). The Weng'an biota and the Ediacaran radiation of multicellular eukaryotes. National Science Review *1*, 498-520.
2. Chen, L., Xiao, S., Pang, K., Zhou, C., and Yuan, X. (2014). Cell differentiation and germ-soma separation in Ediacaran animal embryo-like fossils. Nature *516*, 238-241.
3. Huldtgren, T., Cunningham, J.A., Yin, C., Stampanoni, M., Marone, F., Donoghue, P.C.J., and Bengtson, S. (2011). Fossilized nuclei and germination structures identify Ediacaran "animal embryos" as encysting protists. Science *334*, 1696-1699.
4. Xiao, S., and Knoll, A.H. (2000). Phosphatized animal embryos from the Neoproterozoic Doushantou Formation at Weng'an, Guizhou, South China. Journal of Paleontology *74*, 767-788.
5. Xiao, S., Zhou, C., Liu, P., Wang, D., and Yuan, X. (2015). Phosphatized acanthomorphic acritarchs and related microfossils from the Ediacaran Doushantuo Formation at Weng'an (South China) and their implications for biostratigraphic correlation. Journal of Paleontology *88*, 1-67.
6. dos Reis, M., Thawornwattana, Y., Angelis, K., Telford, Maximilian J., Donoghue, Philip C.J., and Yang, Z. (2015). Uncertainty in the timing of origin of animals and the limits of precision in molecular timescales. Current Biology *25*, 2939-2950.
7. Xiao, S., Yuan, X., and Knoll, A.H. (2000). Eumetazoan fossils in terminal Proterozoic phosphorites? Proceedings of the National Academy of Sciences, USA *97*, 13684-13689.
8. Chen, J.-Y., Bottjer, D.J., Oliveri, P., Dornbos, S.Q., Gao, F., Ruffins, S., Chi, H., Li, C.W., and Davidson, E. (2004). Small bilaterian fossils from 40 and 55 million years before the Cambrian. Science *305*, 218-222.
9. Xiao, S., Zhang, Y., and Knoll, A.H. (1998). Three-dimensional preservation of algae and animal embryos in a Neoproterozoic phosphate. Nature *391*, 553-558.
10. Chen, J.-Y., Bottjer, D.J., Li, G., Hadfield, M.G., Gao, F., Cameron, A.R., Zhang, C.-Y., Xian, D.-C., Tafforeau, P., Liao, X., et al. (2009). Complex embryos displaying bilaterian characters from Precambrian Doushantuo phosphate deposits, Weng'an, Guizhou, China. Proceedings of the National Academy of Sciences *106*, 19056–19060.
11. Chen, J.Y., Bottjer, D.J., Davidson, E.H., Dornbos, S.Q., Gao, X., Yang, Y.H., Li, C.W., Li, G., Wang, X.Q., Xian, D.C., et al. (2006). Phosphatized polar lobe-forming embryos from the Precambrian of Southwest China. Science *312*, 1644-1646.
12. Chen, J., Oliveri, P., Li, C.-W., Zhou, G.-Q., Gao, F., Hagadorn, J.W., Peterson, K.J., and Davidson, E.H. (2000). Precambrian animal diversity: putative phosphatised embryos from the

Doushantuo Formation of China. Proceedings of the National Academy of Sciences, USA *97*, 4457-4462.

13. Cunningham, J.A., Thomas, C.-W., Bengtson, S., Kearns, S.L., Xiao, S., Marone, F., Stampanoni, M., and Donoghue, P.C.J. (2012). Distinguishing geology from biology in the Ediacaran Doushantuo biota relaxes constraints on the timing of the origin of bilaterians. Proceedings of the Royal Society B: Biological Sciences *279*, 2369-2376.
14. Bengtson, S., Cunningham, J.A., Yin, C., and Donoghue, P.C.J. (2012). A merciful death for the "earliest bilaterian," Vernanimalcula. Evolution & Development *14*, 421-427.
15. Zhang, X.-G., and Pratt, B.R. (2014). Possible algal origin and life cycle of Ediacaran Doushantuo microfossils with dextral spiral structure. Journal of Palaeontology *88*, 92-98.
16. Butterfield, N.J. (2011). Terminal Developments in Ediacaran Embryology. Science *334*, 1655-1656.
17. Hagadorn, J.W., Xiao, S.H., Donoghue, P.C.J., Bengtson, S., Gostling, N.J., Pawlowska, M., Raff, E.C., Raff, R.A., Turner, F.R., Chongyu, Y., et al. (2006). Cellular and subcellular structure of Neoproterozoic animal embryos. Science *314*, 291-294.
18. Cunningham, J.A., Vargas, K., Pengju, L., Belivanova, V., Marone, F., Martinez-Perez, C., Guizar-Sicairos, M., Holler, M., Bengtson, S., and Donoghue, P.C.J. (2015). Critical appraisal of tubular putative eumetazoans from the Ediacaran Weng'an Doushantuo biota. Proceedings of the Royal Society B-Biological Sciences *282*, 158-166.
19. Donoghue, P.C.J., Bengtson, S., Dong, X.-P., Gostling, N.J., Huldtgren, T., Cunningham, J.A., Yin, C., Yue, Z., Peng, F., and Stampanoni, M. (2006). Synchrotron X-ray tomographic microscopy of fossil embryos. Nature *442*, 680-683.
20. Yin, Z., Zhao, D., Pan, B., Zhao, F., Zeng, H., Li, G., and Zhu, M. (2018). Early Cambrian animal diapause embryos revealed by X-ray tomography. Geology *46*, 387–390.
21. Cunningham, J.A., Vargas, K., Yin, Z., Bengtson, S., and Donoghue, P.C.J. (2017). The Weng'an Biota (Doushantuo Formation): an Ediacaran window on soft-bodied and multicellular microorganisms. Journal of the Geological Society *174*, 793–802.
22. Xiao, S., Zhou, C., and Yuan, X. (2007). Undressing and redressing Ediacaran embryos. Nature *446*, E9-E10.
23. Raff, E.C., Villinski, J.T., Turner, F.R., Donoghue, P.C.J., and Raff, R.A. (2006). Experimental taphonomy shows the feasibility of fossil embryos. Proceedings of the National Academy of Sciences, USA *103*, 5846-5851.

24. Xiao, S., Knoll, A.H., Yuan, X., and Pueschel, C.M. (2004). Phosphatized multicellular algae in the Neoproterozoic Doushantuo Formation, China, and the early evolution of florideophyte red algae. Am. J. Bot. *91*, 214-227.

25. Yin, Z., Cunningham, J.A., Vargas, K., Bengtson, S., Zhu, M., and Donoghue, P.C.J. (2017). Nuclei and nucleoli in embryo-like fossils from the Ediacaran Weng'an Biota. Precambrian Research *301*, 145-151.

26. Sanchis, D., Carrasco, D., and Quesada, A. (2004). The genus *Microcystis* (Microcystaceae/Cyanobacteria) from a Spanish reservoir: A contribution to the definition of morphological variations. Nova Hedwigia *79*, 479-495.

27. Otsuka, S., Suda, S., Li, R., Matsumoto, S., and Watanabe, M.M. (2000). Morphological variability of colonies of *Microcystis* morphospecies in culture. Journal of General and Applied Microbiology *46*, 39-50.

28. Šejnohová, L., and Maršálek, B. (2012). *Microcystis*. In Ecology of Cyanobacteria II. Their diversity in space and time. (Springer), pp. 195-228.

29. Xiao, M., Willis, A., Burford, M.A., and Li, M. (2017). Review: a meta-analysis comparing cell-division and cell-adhesion in Microcystis colony formation. Harmful Algae *67*, 85-91.

30. Liu, L., Huang, Q., and Qin, B. (2018). Characteristics and roles of *Microcystis* extracellular polymeric substances (EPS) in cyanobacterial blooms: a short review. Journal of Freshwater Ecology *33*, 183-193.

31. Hutchison, E.A., Miller, D.A., and Angert, E.R. (2014). Sporulation in bacteria: beyond the standard model. In The bacterial spore: from molecules to systems, Volume 2, 2015/06/25 Edition, P. Eichenberger and A. Driks, eds. (Wasgingtson, DC: American Society for Microbiology), pp. 87-102.

32. Xiao, S. (2002). Mitotic topologies and mechanics of Neoproterozoic algae and animal embryos. Paleobiology *28*, 244-250.

33. Xiao, S., Knoll, A.H., Schiffbauer, J.D., Zhou, C., and Yuan, X. (2012). Comment on "Fossilized nuclei and germination structures identify Ediacaran 'animal embryos' as ecysting protists". Science *335*, 1169.

34. Rensing, S.A. (2016). (Why) Does Evolution Favour Embryogenesis? Trends in Plant Science *21*, 562-573.

35. Cunningham, J.A., Vargas, K., Yin, Z., Bengtson, S., and Donoghue, P.C.J. (2017). The Weng'an Biota (Doushantuo Formation): an Ediacaran window on soft-bodied and multicellular microorganisms. Journal of the Geological Society *174*, 793-802.

36. Choi, K.-S., and Park, K.-I. (2010). Review on the protozoan parasite *Perkinsus olseni* (Lester and Davis 1981) infection in Asian waters. In Coastal environmental and ecosystem issues of the East China Sea, A. Ishimatsu and H.-J. Lie, eds. (Nagasaki: Terrapub and Nagasaki University), pp. 269-281.

37. Azevedo, C., Corral, L., and Cachola, R. (2009). Fine structure of zoosporulation in *Perkinsus atlanticus* (Apicomplexa: Perkinsea). Parasitology *100*, 351-358.

38. Barsanti, L., and Gualtieri, P. (2014). Algae: anatomy, biochemistry, and biotechnology, (Boca Raton: CRC Press).

39. Krishnamurthy, V. (2001). Reproductive biology of eukaryotic algae. In Reproductive biology of plants, B.M. Johri and P.S. Srivastava, eds. (Berlin: Springer, Heidelberg), pp. 57-95.

40. Rusig, A.-M., Ouichou, A., Le Guyader, H., and Ducreux, G. (2001). Ontogenesis in the Fucophyceae: case studies and comparison of fucoid zygotes and *Sphacelaria* apical cells. Cryptogamie, Algologie *22*, 227-248.

41. Michetti, K.M., Martín, L.A., and Leonardi, P.I. (2013). Carpospore release and sporeling development in Gracilaria gracilis (Gracilariales, Rhodophyta) from the southwestern Atlantic coast (Chubut, Argentina). Journal of Applied Phycology *25*, 1917-1924.

42. Wang, G., Jiang, C., Wang, S., Wei, X., and Zhao, F. (2012). Early development of *Grateloupia turuturu* (Halymeniaceae, Rhodophyta). Chinese Journal of Oceanology and Limnology *30*, 264-268.

43. Brawley, S.H., Wetherbee, R., and Quatrano, R.S. (1976). Fine-structural studies of the gametes and embryo of *Fucus vesiculosus* L. (Phaeophyta). II. The cytoplasm of the egg and young zygote. Journal of Cell Science *20*, 255-271.

44. Tsekos, I. (1983). The Ultrastructure of Carposporogenesis in Gigartina teedii (Roth) Lamour. (Gigartinales, Rhodophyceae): Gonimoblast Cells and Carpospores. Flora *174*, 191-211.

45. Kirk, D.L. (2000). *Volvox* as a model system for studying the ontogeny and phylogeny of multicellularity and cellular differentiation. Journal of Plant Growth Regulation *19*, 265-274.

46. Smith, G.M. (1944). A comparative study of the species of *Volvox*. Transactions of the American Microscopical Society *63*, 265-310.

47. Arakaki, Y., Kawai-Toyooka, H., Hamamura, Y., Higashiyama, T., Noga, A., Hirono, M., Olson, B.J., and Nozaki, H. (2013). The simplest integrated multicellular organism unveiled. PLoS One *8*, e81641.

48. Sebe-Pedros, A., Degnan, B.M., and Ruiz-Trillo, I. (2017). The origin of Metazoa: a unicellular perspective. Nat Rev Genet *18*, 498-512.

49. Ondracka, A., Dudin, O., and Ruiz-Trillo, I. (2018). Decoupling of nuclear division cycles and cell size during the coenocytic growth of the ichthyosporean *Sphaeroforma arctica*. Currrent Biology *28*, 1964-1969 e1962.
50. Suga, H., and Ruiz-Trillo, I. (2013). Development of ichthyosporeans sheds light on the origin of metazoan multicellularity. Dev Biol *377*, 284-292.
51. Marshall, W.L., and Berbee, M.L. (2010). Facing unknowns: living cultures (*Pirum gemmata* gen. nov., sp. nov., and A*beoforma whisleri*, gen. nov., sp. nov.) from invertebrate digestive tracts represent an undescribed clade within the unicellular opisthokont lineage Ichthyosporea (Mesomycetozoea). Protist *132*, 33-57.
52. Dudin, O., Ondracka, A., Grau-Bové, X., A.B. Haraldsen, A., Toyoda, A., Suga, H., Bråte, J., and Ruiz-Trillo, I. (2019). A unicellular relative of animals generates an epithelium-like cell layer by actomyosin dependent cellularization. bioRxiv.
53. Kraus, Y.A. (2006). Morphomechanical programming of morphogenesis in Cnidarian embryos. International Journal of Developmental Biology *50*, 267-275.
54. Komatsu, M. (1976). Wrinkled blastula of the sea-star, *Asterina minor* Hayashi. Development, Growth and Differentiation *18*, 435-438.
55. Kraus, Y., Flici, H., Hensel, K., Plickert, G., Leitz, T., and Frank, U. (2014). The embryonic development of the cnidarian Hydractinia echinata. Evol Dev *16*, 323-338.
56. Sebé-Pedrós, A., Degnan, B.M., and Ruiz-Trillo, I. (2017). The origin of Metazoa: a unicellular perspective. Nature Reviews Genetics *18*, 498-512.
57. Sebé-Pedrós, A., de Mendoza, A., Lang, B.F., Degnan, B.M., and Ruiz-Trillo, I. (2011). Unexpected repertoire of metazoan transcription factors in the unicellular holozoan *Capsaspora owczarzaki*. Molecular Biology and Evolution *28*, 1241-1254.
58. Dickinson, D.J., Nelson, W.J., and Weis, W.I. (2012). An epithelial tissue in *Dictyostelium* challenges the traditional origin of metazoan multicellularity. Bioessays *34*, 833-840.
59. Nakanishi, N., Sogabe, S., and Degnan, B.M. (2014). Evolutionary origin of gastrulation: insights from sponge development. BMC Biology *12*, 26.
60. Li, C., Cheng, M., Zhu, M., and Lyons, T.W. (2018). Heterogeneous and dynamic marine shelf oxygenation and coupled early animal evolution. Emerging Topics in Life Sciences *2*, 279-288.
61. Team, R.C. (2016). R: A language and environment for statistical computing. (Vienna, Austria: R Foundation for Statistical Computing).

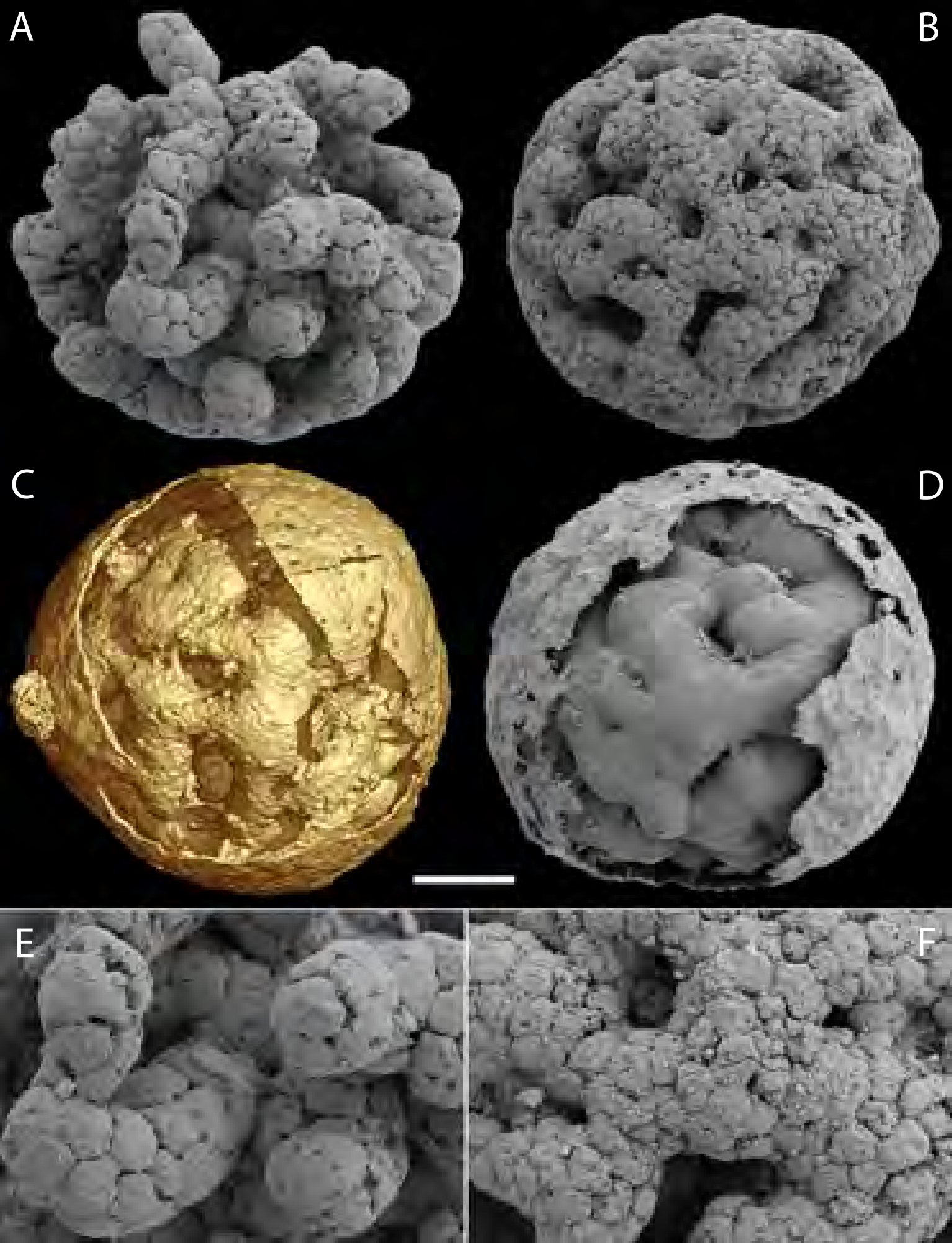
A
B
C
D
E
F

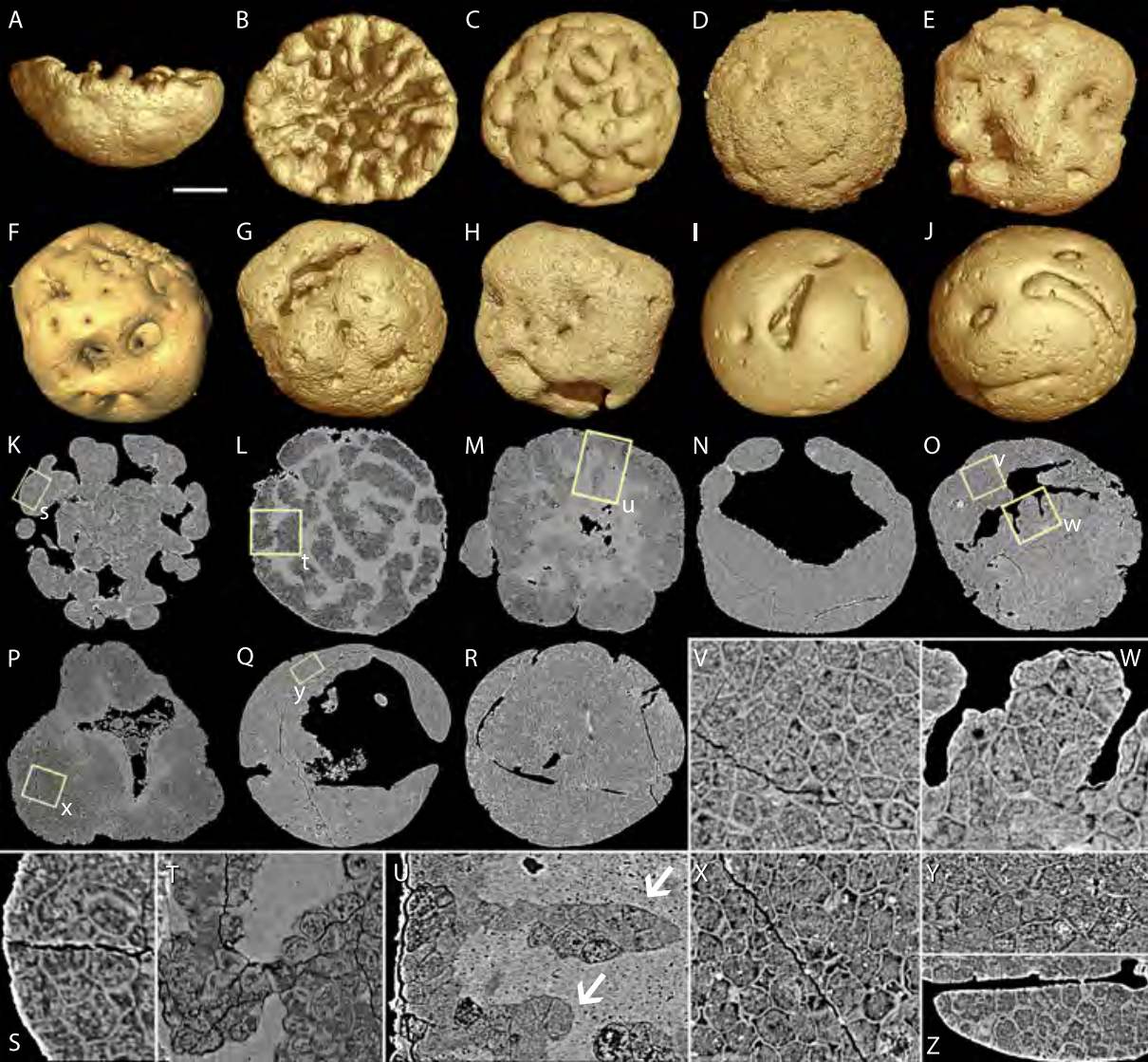
A
B
C
D
E
F
G
H
I
J
K
L
M
N
O
s
t
u
v
w
P
Q
R
x
y
V
W
S
T
U
X
Y
Z

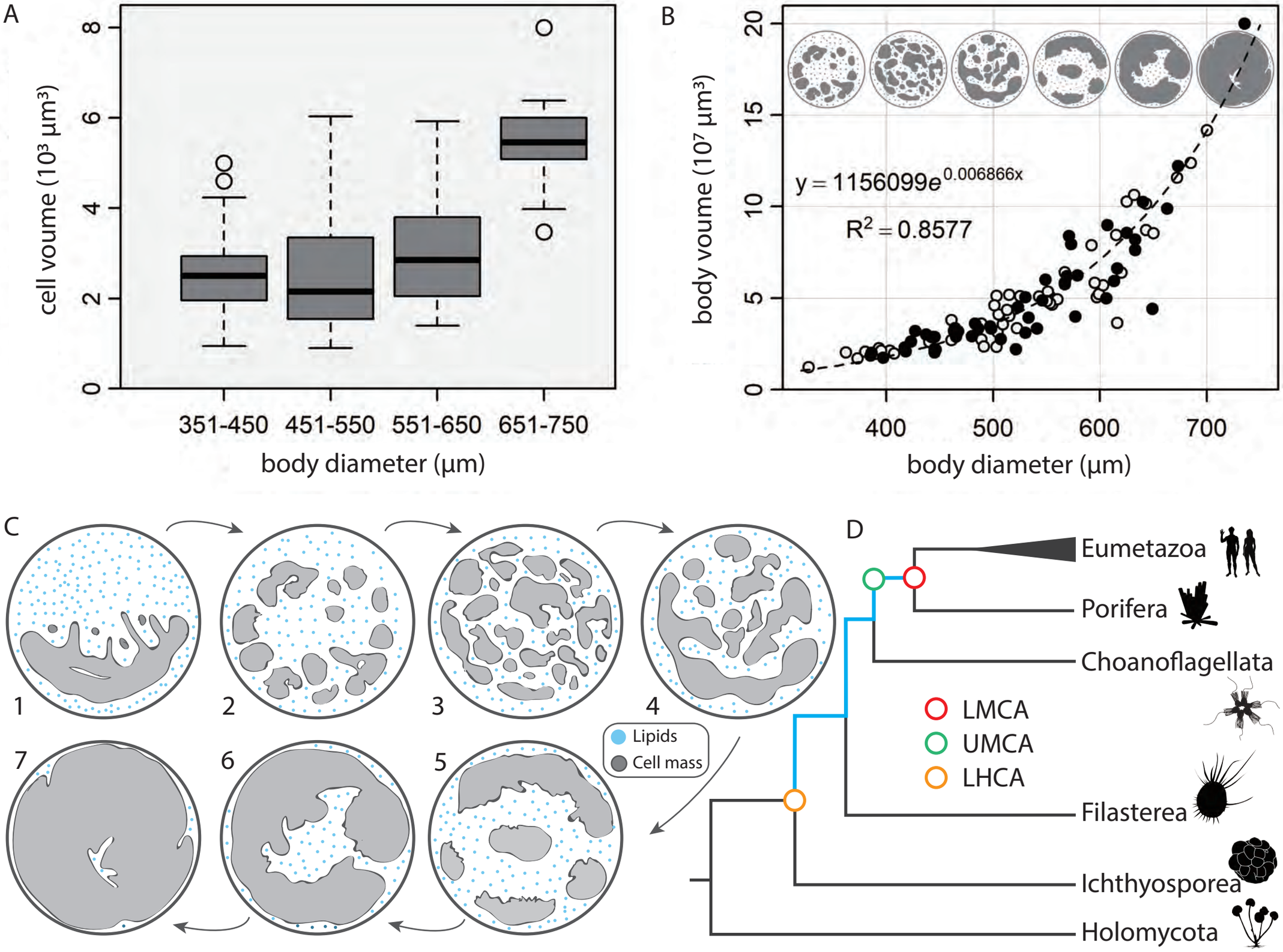
A
cell voume (10³ µm³)
0
2
4
6
8
351-450
451-550
551-650
651-750
body diameter (µm)
B
body voume (10⁷ µm³)
0
5
10
15
20
y = 1156099e^0.006866x
R² = 0.8577
400
500
600
700
body diameter (µm)
C
1
2
3
4
5
6
7
Lipids
Cell mass
D
Eumetazoa
Porifera
Choanoflagellata
LMCA
UMCA
LHCA
Filasterea
Ichthyosporea
Holomycota

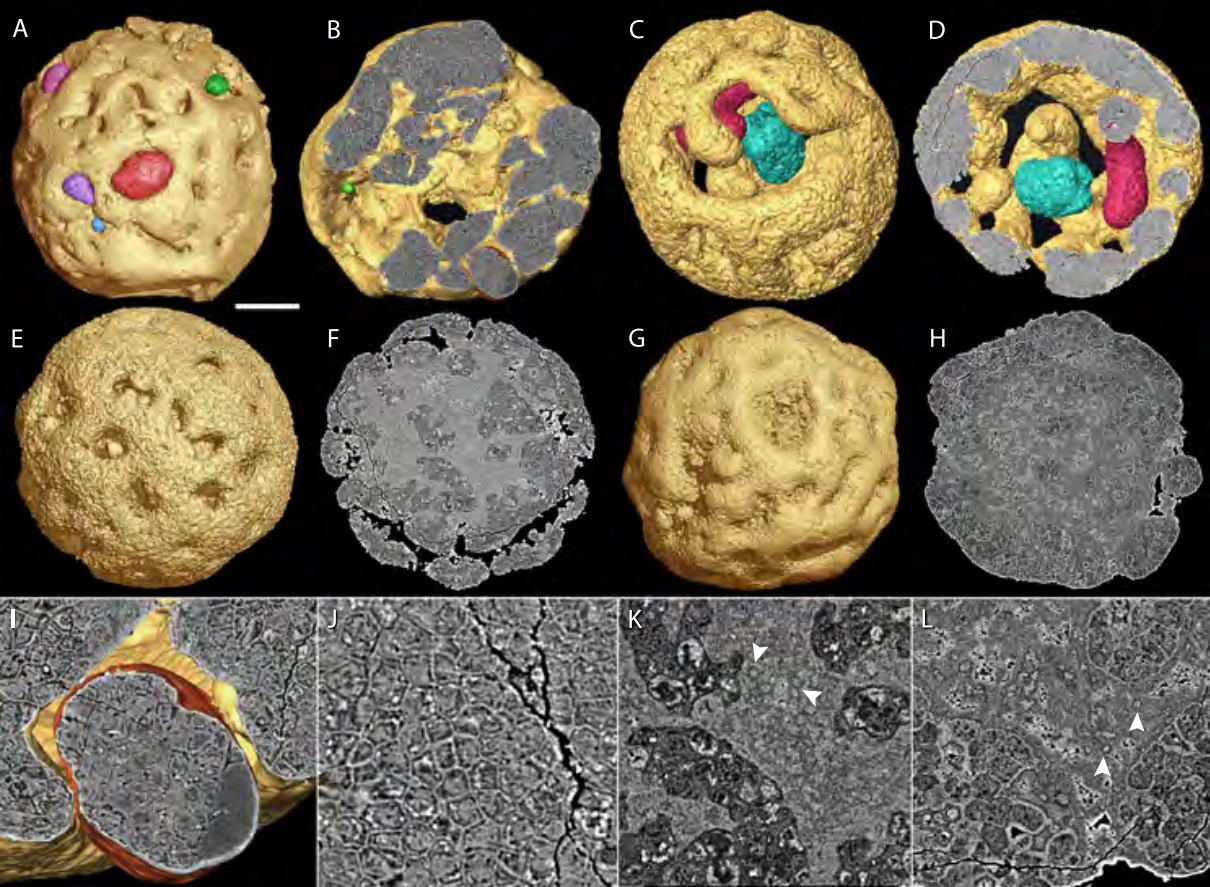
A
B
C
D
E
F
G
H
I
J
K
L

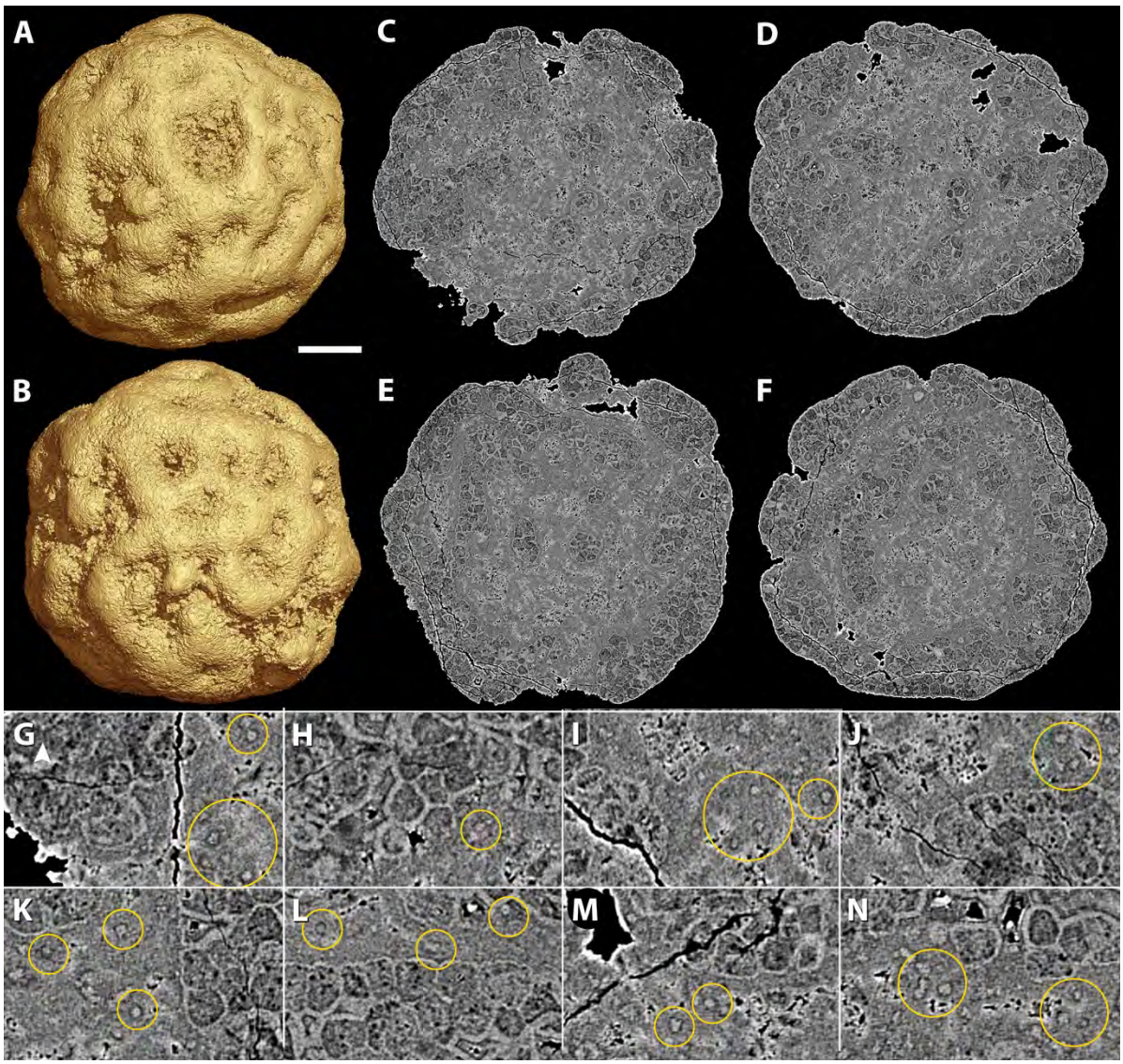

Figure S1. Specimens with envelopes. Related to Figure 1.

(A-D, L), Surface renderings, (A-D) are different views of the same specimens, respectively. (E-H), Virtual slices of (A-D), respectively. (I-K), Scanning electron microscopic images. The envelopes in (C, D) and (I) are ornamented, the others are smooth. Scale bar: 85µm for (A, B), 130µm for (C, D), 80µm for (E, F), 110µm for (G, H), 95µm for (I), 90µm for (J), 100µm for (K), 105 µm for (l).

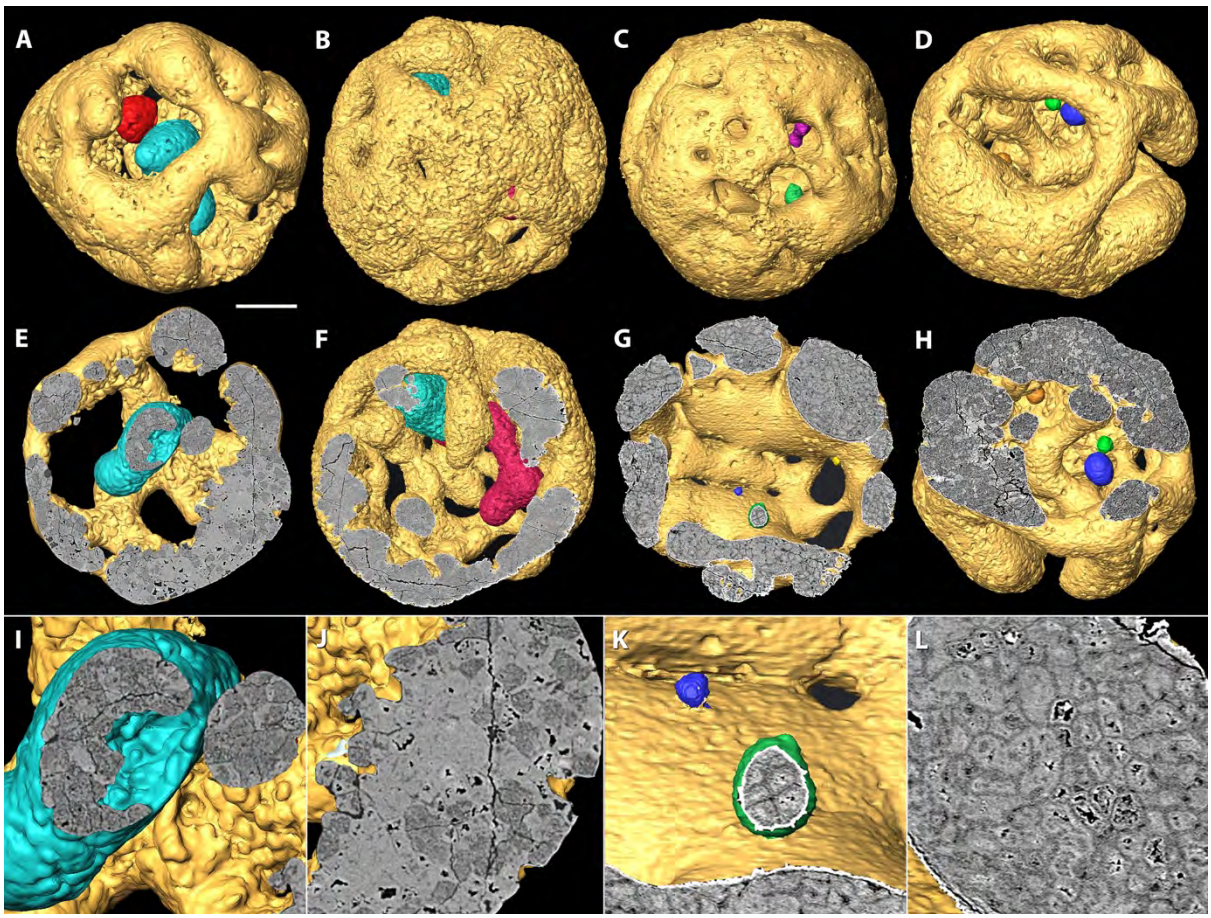

Figure S2. *Caveasphaera* fossils with isolated cell clusters. Related to Figure 2.

(A-D), Volume renderings with the isolated cell clusters indicated by red, cyan, green and blue. (E, H), Three-dimensional virtual sections of (A-D), respectively, showing the distribution of the isolated cell clusters trapped in the cage. (I, J) and (K-L) close-up views of (E) and(G), respectively, showing cellular structure. Scale bar: 100µm for (A, E), 105µm for (B, F), 140µm for (C), 130µm for (G), 120µm for (D, H), 35µm for (I-L).

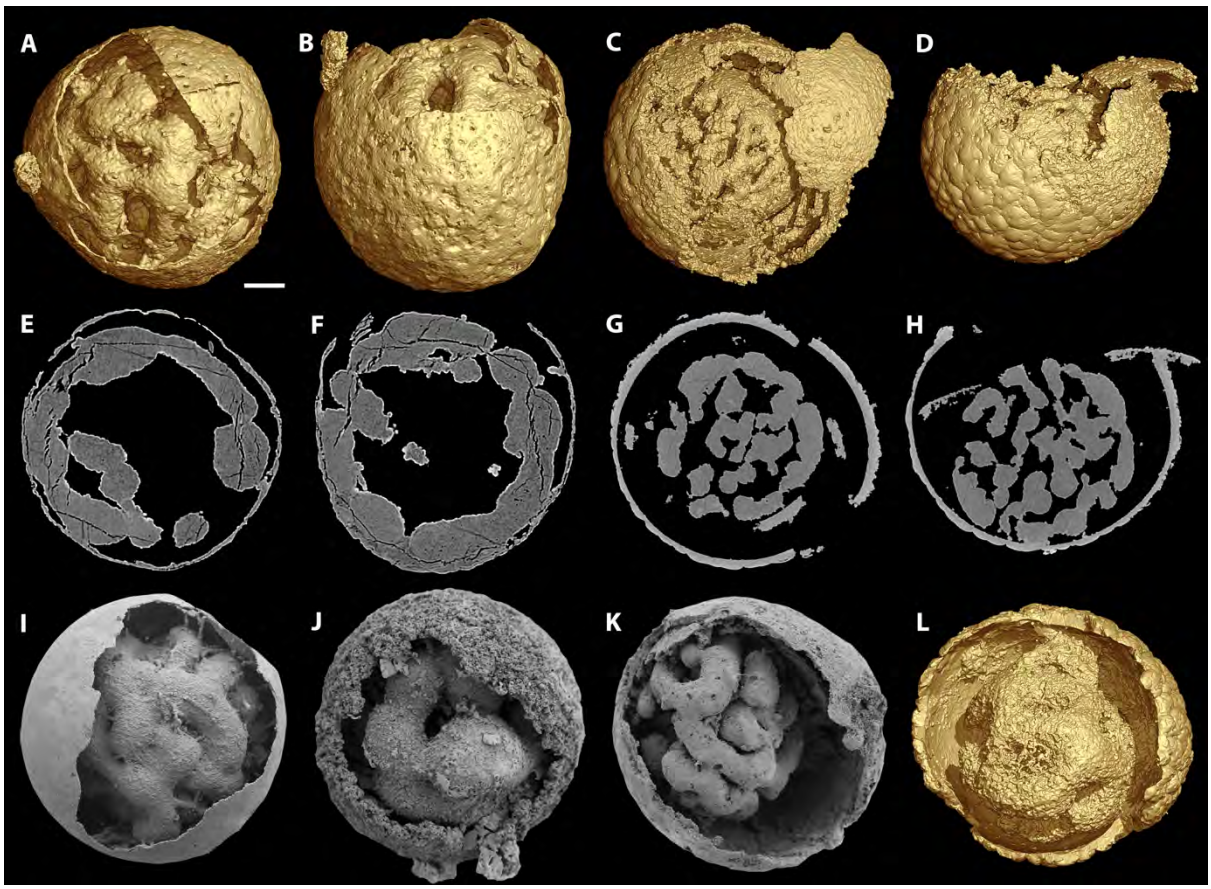

Figure S3. *Caveasphaera* with intercellular matrix preserved. Related to Figure 4.

(A, B), Surface renderings of the same specimen with different views. (C-F), Virtual slices from different directions and depths, showing cellular branches and fossilized intercellular matrix. (G-N), Close-up views of (C-F), with the circles indicating the lipid-like vesicles within the intercellular matrix. Scale bar: 100μm for (A-F), 25μm for (G-N).